

Universal pulses for superconducting qudit ladder gates

Boxi Li,^{1,2,*} F. A. Cárdenas-López,¹ Adrian Lupascu,³ and Felix Motzoi^{1,2,†}

¹*Forschungszentrum Jülich, Institute of Quantum Control (PGI-8), D-52425 Jülich, Germany*

²*Institute for Theoretical Physics, University of Cologne, D-50937 Cologne, Germany*

³*Institute for Quantum Computing, Department of Physics and Astronomy, and Waterloo Institute for Nanotechnology, University of Waterloo, Waterloo, Ontario, Canada N2L 3G1*

Qudits, generalizations of qubits to multi-level quantum systems, offer enhanced computational efficiency by encoding more information per lattice cell, avoiding costly swap operations and providing even exponential speedup in some cases. Utilizing the d -level manifold, however, requires high-speed gate operations because of the stronger decoherence at higher levels. While analytical control methods have proven effective for qubits in achieving fast gates with minimal control errors, their extension to qudits is nontrivial due to the increased complexity of the energy level structure arising from additional ancillary states. In this work, we present a universal pulse construction for generating rapid, high-fidelity unitary rotations between adjacent qudit levels, thereby providing a prescription for any gate in $SU(d)$. Control errors in these operations are effectively analyzed within a four-level subspace, including two leakage levels with approximately opposite detuning. By identifying the optimal degrees of freedom, we derive concise analytical pulse schemes that suppress multiple control errors and outperform existing methods. Remarkably, our approach achieves consistent coherent error scaling across all levels, approaching the quantum speed limit independently of parameter variations between levels. Validation on transmon circuits demonstrates significant improvements in gate fidelity for various qudit sizes aiming for 10^{-4} error. This method provides a scalable solution for improving qudit control and can be broadly applied to other quantum systems with ladder structures or operations involving multiple ancillary levels.

I. INTRODUCTION

Quantum computation and quantum information processing protocols often rely on qubits, or two-level systems, as the fundamental units of computation due to their simplicity and close analogy to classical computing. However, most quantum systems comprise more than just two levels. These additional quantum levels can also be used as an information register, which is known as a qudit, a generalization of the qubit to a d -level system. Exploring the full Hilbert space of qudits enables more efficient computation by increasing the amount of information stored per quantum unit.

Qudit-based quantum computation offers several known advantages over qubit-based approaches. For instance, a d -level system can encode $\log_2(d)$ qubits [1]. This has been exploited for efficient compilation of arbitrary unitaries, requiring an exponentially reduced number of circuit layers [2–6], to simulate bosonic modes for studying light-matter processes [7, 8] and lattice gauge theories [9–11], for enhancing the robustness in quantum cryptography [12, 13], and for simplified implementation of quantum error correction protocols [14–16]. In general, the larger density of registers means that the connectivity of qubit-based architectures is increased, since neighbouring qudits can share up to d^2 level couplings. Qudit processors have been implemented across various physical platforms, including trapped-ions [17–20], Rydberg atoms [21], ultracold atomic mixtures [22], molecu-

lar spins [23, 24], photonic systems [25–29] and superconducting circuits [30–37]; such implementations contribute to significant progress on qudit-based quantum computation.

Despite these advancements, maintaining coherent control of all the qudit levels poses complex new challenges. In transmon superconducting circuits, where the quantum system is represented by a non-linear oscillator [38], each qudit operation needs to be addressed differently due to the varying surrounding level structure. Compared to a qubit operation, the presence of additional leakage channels significantly, limits the gate performance, as shown in Fig. 1a-c. For instance, it has been reported that the gate time of a single-qudit gate is around 30 ns [31, 33, 35], which is three times longer than that required for single-qubit gates with state-of-the-art quantum control techniques [39]. Therefore, developing quantum control protocols for qudits is crucial for making qudit computation practical. Of particular relevance is the Derivative Removal by Adiabatic Gate (DRAG) method [40–43], successfully employed in superconducting qubit systems to reduce leakage and phase errors. DRAG’s simplicity and flexibility allow engineering efficient pulses with easy-to-calibrate parameters, making it ubiquitous in the superconducting qubits platform [39, 44–47]. The same advantages remain even with the presence of multiple error sources, whereby multiple DRAG corrections can be combined, offering efficient yet compact solutions [42, 48].

In this article, we extend the DRAG framework to engineer universally applicable and high-precision analytical control pulses for qudit systems within a ladder structure. The ladder gateset that connects levels k and $k + 1$ is suf-

* b.li@fz-juelich.de

† f.motzoi@fz-juelich.de

ficient for universal gates within the qubit. We show that porting the widely-used single-derivative DRAG method, as previously suggested in [41] and experimentally implemented in [32, 49], offers little benefit in the qudit case because it is overconstrained in removing multiple leakage channels. To address this, we introduce a recursive DRAG approach that incorporates higher-order derivatives, providing new degrees of freedom that are used to suppress both single- and multi-photon errors. Our systematic study conducted on a transmon circuit across various qudit sizes demonstrates that higher-level control can be designed within a variable four-level subspace involving two nearest-neighbour interactions. Despite the presence of multiple parameters in the circuit description, we find a universal behaviour in the pulse-specific quantum speed limits. In particular, the speed limits collapse to the same times irrespective of all but one system parameter, but are strongly dependent on whether certain multi-photon transitions are suppressed. We observe significant improvements in gate performance and successfully reduce gate times to mitigate dephasing caused by voltage fluctuations during gate implementation. These results are broadly applicable to any qudit platform with multiple connected ancillary levels.

In the following, we start with the transmon model and derive the four-level effective Hamiltonian in Section II. Next, we introduce and explore the recursive DRAG method in detail and perform a systematic study of its performance in Section III. Significant improvement in fidelity is observed across a wide range of parameters, with a universal behaviour across all levels independent of parameter variations between levels. In Section IV, we discuss other potential control errors beyond the two-level transition and provide a summary of our findings in Section V.

II. QUDIT MODEL FOR UNIVERSAL QUANTUM GATES

A. Native gate set for superconducting qudit

Our objective is that, for a transmon system, each individual ladder transition between adjacent states, $|k\rangle$ and $|k+1\rangle$, can be selectively controlled. This allows arbitrary unitaries on $SU(d)$ to be implemented. Since a calibrated $\pi/2$ gate combined with a virtual Z gate [50] is a complete native gate set, as we show in Appendix A, our primary focus in the following study is on the $\pi/2$ gate. In addition, we also present results for the π gate, which represents the most challenging Givens rotation for a fixed gate duration due to its requirement for the strongest drive. Overall, these methods can be extended to rotations of arbitrary angles, which can be very helpful for reducing circuit compilation depths [51].

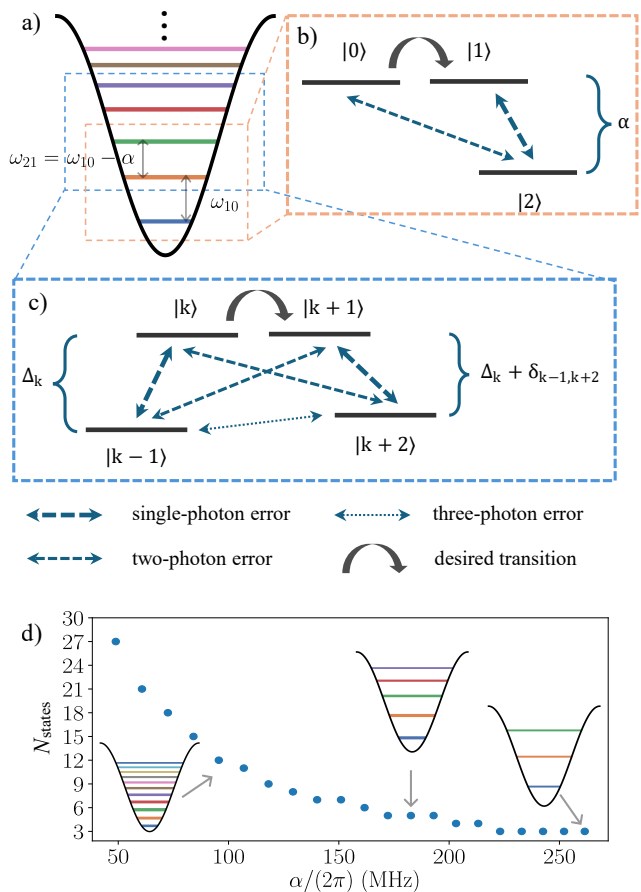


FIG. 1. Energy structure of driving a two-level transition in a qudit system. (a) Typical energy structure of a transmon system. Energy levels and error transitions for (b) the ground and first excited states, and (c) general ladder transition between higher levels in the rotating frame. (d) The number of levels that can be used as a qudit quantum register as a function of the anharmonicity. The upper bound is set by the decoherence introduced by charge fluctuations. The detailed discussion can be found in Appendix B.

B. The transmon Hamiltonian

In this subsection, we derive the effective Hamiltonian for selectively driving the $|k\rangle \leftrightarrow |k+1\rangle$ transition in a superconducting transmon. A transmon nonlinear oscillator is described by the following Hamiltonian [38]

$$\hat{H} = 4E_C[\hat{n} - n_g(t)]^2 - E_J \cos(\hat{\varphi}) \quad (1)$$

where E_C and E_J represent the charge and Josephson energies, respectively, and $n_g(t)$ is the dimensionless gate voltage. The operator \hat{n} is the charge operator, indicating the number of Cooper pairs on the island, and $\hat{\varphi}$ denotes the phase operator. For implementing single-qudit operations, we capacitively drive the transmon using $n_g(t) = n_0(t) \cos(\omega_d t)$ resulting in the Hamiltonian

$$\hat{H}_{\text{ctrl}} = \Omega(t) \cos(\omega_d t) \hat{n} \quad (2)$$

where $\Omega(t) = -8E_C n_0(t)$ is the drive envelope, and ω_d is the drive frequency.

When only the lowest few energy levels are considered, the transmon can be modelled as an approximate Duffing oscillator [52, 53]. In this model, the control operator is expressed as $\hat{n} \propto (\hat{b}^\dagger + \hat{b})$, where \hat{b} is the annihilation operator of a linear oscillator. Consequently, the control Hamiltonian adopts a ladder configuration, connecting states $|k\rangle \leftrightarrow |k \pm 1\rangle$. The transmon Hamiltonian without external drive then simplifies to

$$\hat{H}_0^{\text{duf}} = \omega_q \hat{b}^\dagger \hat{b} + \frac{\alpha}{2} \hat{b}^\dagger \hat{b}^\dagger \hat{b} \hat{b}, \quad (3)$$

with $\omega_q = \sqrt{8E_J E_C} - E_C$ and $\alpha = -E_C$. As long as the states are in the potential well, the dominant coupling is still this ladder coupling between the adjacent levels, as will be shown later. However, the eigenenergies and coupling strengths deviate from the Duffing model at higher levels due to the higher-order expansion of the cosine term in Eq. (1) [52].

An accurate effective model requires exact diagonalization up to a truncation level N_{max} , which gives

$$H_0 = \sum_{k=0}^{N_{\text{max}}} \omega_k |k\rangle, \quad (4)$$

and for the charge operator:

$$\hat{n} = \sum_{k=0}^{N_{\text{max}}-1} \left[n_{k,k+1} |k\rangle\langle k+1| + \sum_{j=1} n_{k,k+2j+1} |k\rangle\langle k+2j+1| \right] + \text{h.c.} \quad (5)$$

Unlike the Duffing oscillator model, the \hat{n} operator in the effective frame exhibits additional transitions, these non-zeros matrix elements are related to the underlying parity symmetry from the Mathieu functions, the formal solution of the Hamiltonian in Eq. (1). Here, we distinguish between the ladder coupling between $|k\rangle \leftrightarrow |k+1\rangle$ and high-order couplings. The latter are typically orders of magnitude smaller and are suppressed by the rotating wave approximation, as we will demonstrate later.

From this point, it is more convenient to express the Hamiltonian in the rotating frame defined by the transformation $R = \exp(-i\omega_d t \sum_k k |k\rangle\langle k|)$, where ω_d is the selected driving transition frequency. This leads to the following total Hamiltonian:

$$\hat{H} = \sum_{k=0}^{N_{\text{max}}} \tilde{\Delta}_k \hat{\Pi}_k + \Omega(t) \cos(\omega_d t) \left[\sum_{k=0}^{N_{\text{max}}-1} \sum_{j=1} n_{k,k+2j+1} |k\rangle\langle k+2j+1| e^{(2j+1)i\omega_d t} + \sum_{k=0}^{N_{\text{max}}-1} n_{k,k+1} |k\rangle\langle k+1| e^{i\omega_d t} + \text{h.c.} \right], \quad (6)$$

where $\tilde{\Delta}_k = \omega_k - k\omega_d$ is the detuning between the k -th level with the k -th driving frequency harmonic. The maximal j is chosen such that $k+2j+1$ falls within the truncated levels. In the rotating frame, the coupling terms oscillate rapidly except for the ladder coupling between $|k\rangle \leftrightarrow |k+1\rangle$. Therefore, we can neglect these rapidly oscillating terms within the rotating wave approximation (RWA), leading to

$$\hat{H}_{\text{rwa}} = \sum_{k=0}^{N_{\text{max}}} \tilde{\Delta}_k \hat{\Pi}_k + \frac{\Omega(t)}{2} \sum_{k=0}^{N_{\text{max}}-1} (n_{k,k+1} |k\rangle\langle k+1| + \text{h.c.}) \quad (7)$$

In this Hamiltonian, we recover the desired ladder coupling, albeit with renormalized eigenenergies and coupling strengths. To target a specific ladder transition $(k, k+1)$, the drive frequency is chosen such that $\tilde{\Delta}_k = \tilde{\Delta}_{k+1}$ for the desired k . The nonlinearity, captured by the remaining $\tilde{\Delta}_k - \tilde{\Delta}_j$ for $j \notin \{k, k+1\}$, permits selective driving of any transition between neighbouring levels.

In addition to the Hamiltonian, we also consider the possible decoherence of the higher levels. To use the quantum states as a qudit, we demand that they are robust against charge fluctuations, which increase exponentially up the ladder. This condition sets an upper bound on the maximal number of usable states N_{states} , which a priori depends on the ratio E_J/E_C , and is graphed in Fig. 1d as a function of anharmonicity $\alpha \approx -E_C$. A higher E_J corresponds to a deeper potential, allowing for more confined states, while a lower E_C reduces charge fluctuations. However, in such a regime we also have decreases in the frequency difference between transitions, making selective driving more challenging. Instead of using the E_J/E_C ratio, it is more natural to select the usable states in terms of their coherence times T_1 and T_ϕ . In our case, as we consider fixed-frequency transmons, the main source of error will correspond to capacitive losses and dephasing due to charge fluctuations. As an optimistic forward-looking estimation, we set the upper bound of T_ϕ for the highest level N_{states} to be around 100 μs such that we are able to potentially achieve gate error below 10^{-4} for a 10 ns gate. For the parameters we choose, this corresponds to a charge dispersion of about 10^{-3} GHz. The details on the calculation of the charge fluctuation and coherence times are presented in Appendix B. In principle, for certain quantum operations, decoherence could be partially mitigated by applying dynamical decoupling methods [54]. In this work, however, we consider more generally using quantum control shaping to speed up the operation time and reduce the irreversible effect of decoherence.

C. Four-level effective model

Although the full qudit has many levels, to drive a $|k\rangle \leftrightarrow |k+1\rangle$ transition many of the states are very far away detuned and thus play little role in the dynamics.

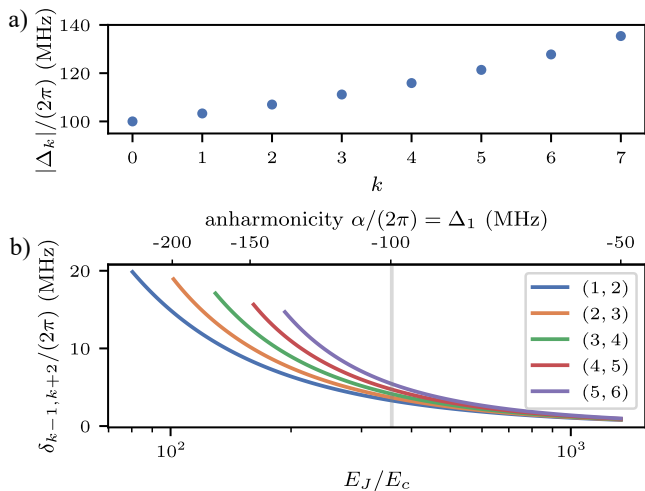


FIG. 2. Properties of transmon qubits. a) Detuning between the target subspace and the leakage levels in the rotating frame. The qubit frequency and anharmonicity of the ground state are 5 GHz and -100 MHz, corresponding to $E_J/E_C \approx 355$. For $k = 0$, $\Delta_k = \alpha$. b) The small energy gap between the two leakage levels $|k-1\rangle$ and $|k+2\rangle$ for the first five transitions. This is much smaller than Δ_k , leading to the energy structure shown in Fig. 1. The grey vertical line marks the parameters used in (a).

Therefore, we focus on nearest-neighbour transitions and further simplify the model to a four-level system. This choice is validated by the numerical simulations that follow. We define $\omega_d = \omega_{k+1} - \omega_k - \delta_d$, with δ_d denoting a designed small detuning between the drive frequency and the energy separation. The special case for qubits, $k = 0$, has been studied over the last decade [55]. The primary control error arises from the coupling to the nearest neighbouring levels, $|k-1\rangle$ and $|k+2\rangle$, as illustrated in Fig. 1c. To simplify the analysis, we truncate the Hamiltonian to a four-level subsystem, described by

$$\hat{H}_k^{(4)} = \begin{pmatrix} \Delta_k & \frac{\lambda_{k-1}\bar{\Omega}_0}{2} & 0 & 0 \\ \frac{\lambda_{k-1}\Omega_0}{2} & \delta_d & \frac{\lambda_k\bar{\Omega}_0}{2} & 0 \\ 0 & \frac{\lambda_k\Omega_0}{2} & 2\delta_d & \frac{\lambda_{k+1}\bar{\Omega}_0}{2} \\ 0 & 0 & \frac{\lambda_{k+1}\Omega_0}{2} & 3\delta_d + \Delta_k + \delta_{k-1,k+2} \end{pmatrix}, \quad (8)$$

where $\bar{\Omega}_0$ denotes the complex conjugate of the complex pulse envelope. For clarity, a constant identity operator has been subtracted.

The two middle levels represent the targeted transition, separated by the small drive detuning δ_d . The first and last levels correspond to the potential leakage levels $|k-1\rangle$ and $|k+2\rangle$. An important observation is that, due to the weak nonlinearity, the level separation between the two leakage levels, $\Delta_k = \omega_{k-1} - 2\omega_k + \omega_{k+1}$, is approximately equal to the anharmonicity $|\alpha|$ and only increases slightly as the levels rise. This is illustrated in Fig. 2a, with the base case $\Delta_0 = \alpha$. The difference between them is given by $\delta_{k-1,k+2} = 3\delta_d - \omega_{k-1} + 3\omega_k - 3\omega_{k+1} + \omega_{k+2}$.

For a harmonic or Duffing oscillator, it is straightforward to verify that $\delta_{k-1,k+2}$ is zero. However, for a transmon oscillator, $\delta_{k-1,k+2}$ takes a small but nonzero value, as illustrated in Fig. 2b, which is plotted as a function of E_J/E_C and the anharmonicity. The curve is truncated when the eigenstate's dispersion noise reaches 10^{-3} GHz, where the qubit coherence time drops below a minimum threshold (see Appendix B). Within this range, the $\delta_{k-1,k+2}$ is much than Δ_k , as depicted in Fig. 1c.

The off-diagonal coupling term in Eq. (8) shows a similar structure as the Duffing model. The term λ_k denotes the renormalized drive strength between level k and $k+1$, given by $\lambda_k = n_{k,k+1}/|n_{0,1}|$, which equals \sqrt{k} in the Duffing approximation. Therefore, the corresponding four-level system has the structure depicted in Fig. 1c. This model holds as long as the state remains within the potential well and the eigenenergy's dispersion to charge noise is sufficiently small.

III. RECURSIVE DRAG PULSE FOR QUDIT GATES

For the lowest two levels in a transmon, $|0\rangle$ and $|1\rangle$, the system reduces to the well-studied single-qubit gate of the transmon qubit. The research on controlling this simple model led to the development of the widely-used DRAG technique [40–43], with a particular focus on minimizing leakage to state $|2\rangle$, as illustrated in Fig. 1b. However, beyond the first two levels, higher-level transitions present different level structure and control errors, as shown in Fig. 1c.

Similar to the well-studied $|0\rangle \leftrightarrow |1\rangle$ transition, residual couplings between the target subspace $|k\rangle$ and $|k+1\rangle$ and the ancillary levels inevitably lead to control errors such as leakage and Stark shifting, especially when attempting to shorten gate times to reduce decoherence. An overview of the error budget is provided in Fig. 3a, indicating the leading contributions. Moreover, to incorporate more levels into the qudit, the nonlinearity $\Delta_k \approx \alpha$ needs to be reduced to protect the state from charge noise (Fig. 1d), which further complicates the control scheme. To address these challenges, we introduce the recursive DRAG pulse, which accelerates gate speeds while maintaining sufficiently low control errors. In the rest of this paper, we demonstrate how the DRAG method can be generalized for higher-level transitions and examine its performance.

A. Single-derivative DRAG and its limitation

The most widely used pulse shape is the single-derivative DRAG pulse [40]

$$\Omega - ia \frac{\dot{\Omega}}{\Delta}, \quad (9)$$

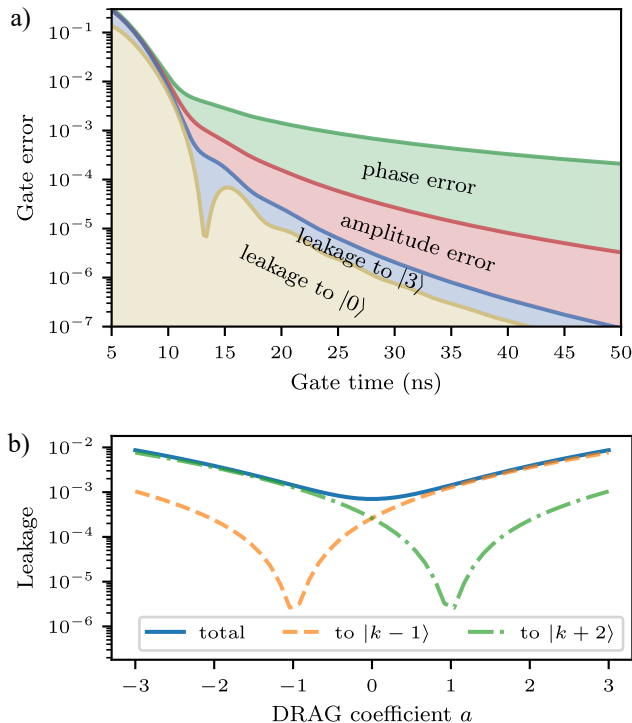


FIG. 3. Control error in driving ladder transitions in a transmon qudit. a) Estimated error budget of driving a $|1\rangle \leftrightarrow |2\rangle$ π rotation using a Hann pulse with an anharmonicity of $\alpha/(2\pi) = -200$ MHz. The phase and amplitude errors are estimated by optimizing with constant detuning and maximal drive amplitude. Note that the error is plotted on a logarithmic scale, e.g., the two leakage errors are of the same order of magnitude. b) The leakage error calculated via Eq. 10 in a regime where the single-derivative DRAG [41] faces limitations and offers no improvement, even with an optimized DRAG coefficient. Parameters used are $\lambda_{k-1} = \lambda_k = \lambda_{k+1} = 1$, $\delta_{k-1,k+2} = 0$ and $t_f = 15$ ns. The pulse is a single-derivative DRAG shape $\Omega - a\dot{\Omega}/\Delta_k$, with Ω the standard Hann pulse.

where a derivative term is introduced to suppress unwanted off-resonant transitions between two levels separated by Δ . In a semiclassical approximation, this approach can be interpreted as engineering a zero point in the spectrum corresponding to Δ [42]. In practice, a free parameter a is often calibrated to account for imperfect knowledge of the Hamiltonian model and higher level error contributions [40, 41]. In addition, a drive with a constant detuning parameter δ_d has been used to correct phase errors, enabling high-fidelity single-qubit gates [39, 42].

However, when driving the $|k\rangle \leftrightarrow |k+1\rangle$ transition in a qudit as described in Eq. (8), both leakage levels $|k+2\rangle$ and $|k-1\rangle$ must be considered. In this case, the single-derivative DRAG as given in Eq. (9), lacks sufficient degrees of freedom to address all sources of error [55]. For instance, if we choose a specific parameter set where $\delta_{k-1,k+2} = 0$ and $\lambda_{k-1} = \lambda_k = \lambda_{k+1} = 1$, the

first derivative term provides no improvement at all, as shown in Fig. 3b, with the leakage population to state $|j\rangle$ defined by

$$\mathcal{L}_j = \frac{1}{4} \sum_{l \in \{k, k+1\}} (|\mathcal{U}_{i,j}|^2 + |\mathcal{U}_{j,l}|^2). \quad (10)$$

This overconstraining occurs because the energy separations for the two leakage levels have opposite signs, i.e., $E_{|k\rangle} - E_{|k-1\rangle} \approx -(E_{|k+2\rangle} - E_{|k+1\rangle})$. This limitation applies to all ladder transitions with $k \geq 1$ in the nonlinear oscillator because $\delta_{k-1,k+2}$ is typically small compared to the anharmonicity (see Fig. 2b).

B. General DRAG correction for a n -photon transition

As shown in Fig. 3, a single degree of freedom is insufficient to simultaneously manage both leakage transitions. To address this limitation, an effective strategy involves incorporating higher-order derivative terms [42, 48]. This approach can be interpreted as a superadiabatic transformation [56], wherein a second adiabatic frame is derived, enabling the introduction of new time-dependent control functions proportional to the second derivative of the original drive shape. In the presence of multiple leakage levels, DRAG corrections can be tailored for each leakage coupling and chained together. In the following, we first present the general formulation and then derive the specific solution to this problem.

For an n th-order coupling $\Omega^n/\Delta_{\text{eff}}^{n-1}$ between two levels separated by Δ , the Hamiltonian in the two-level subspace is given as

$$\hat{H} = -\frac{\Delta}{2} \hat{\sigma}_z + \left(\frac{\Omega^n}{\Delta_{\text{eff}}^{n-1}} \frac{\hat{\sigma}_{jk}^+}{2} + \text{h.c.} \right). \quad (11)$$

Assuming $\Omega^n/\Delta_{\text{eff}}^{n-1} \ll \Delta$, we perform a perturbative expansion with the antihermitian generator $\hat{S}(\tilde{\Omega}) = \frac{\tilde{\Omega}^n}{2\Delta\Delta_{\text{eff}}^{n-1}} \hat{\sigma}_{jk}^+ - \text{h.c.}$ The time-dependent frame transformation is given as

$$\hat{H}'(\Omega) = \hat{V}(\tilde{\Omega}) \hat{H}(g) \hat{V}^\dagger(\tilde{\Omega}) + i \dot{\hat{V}}(\tilde{\Omega}) \hat{V}^\dagger(\tilde{\Omega}) \quad (12)$$

with $\hat{V}(\tilde{\Omega}) = e^{\hat{S}(\tilde{\Omega})}$. This transformation yields

$$\begin{aligned} \hat{H}'(\Omega) &= i \dot{\hat{S}}(\tilde{\Omega}) + \hat{H}(\Omega) + [\hat{S}(\tilde{\Omega}), \hat{H}(\Omega)] + \dots \quad (13) \\ &\approx -\frac{\Delta}{2} \hat{\sigma}_z + \frac{1}{\Delta_{\text{eff}}^{n-1}} \left(\Omega^n - \tilde{\Omega}^n + i \frac{d\tilde{\Omega}^n}{dt} \frac{\tilde{\Omega}^n}{\Delta} \right) \frac{\hat{\sigma}_{jk}^+}{2} \\ &\quad + \text{h.c.}, \end{aligned}$$

where we keep only the leading-order perturbation. Following from the equation above, the DRAG pulse is given by

$$\Omega^n = \tilde{\Omega}^n - i \frac{d\tilde{\Omega}^n}{dt} \frac{\tilde{\Omega}^n}{\Delta}. \quad (14)$$

Therefore, we can derive a drive pulse Ω resistant to this error based on the initial shape Ω and its derivative.

To ensure that the unitary evolution remains consistent under the frame transformation in Eq. (12), it is crucial that the generator \hat{S} vanishes at the beginning and end of the evolution. To achieve this, we use the following initial pulse shape:

$$\Omega_I(t) = \Omega_{\max} \left[\frac{1}{16} \cos \left[6\pi \frac{t}{t_f} \right] - \frac{9}{16} \cos \left[\pi \frac{2t}{t_f} \right] + \frac{1}{2} \right], \quad (15)$$

with t_f the gate time and Ω_{\max} the drive amplitude. For comparison, we also define the widely used Hann pulse:

$$\Omega_{\text{Hann}}(t) = \sin \left[\frac{\pi t}{t_f} \right]^2, \quad (16)$$

which will be used as a baseline to benchmark the control schemes.

C. First-order (linearized) solution for qudits

To manage the two different leakage channels with opposite energy gaps as shown in Fig. 1c and Fig. 3b, two degrees of freedom are required. The leading-order leakage errors in Eq. (8) is associated with the ladder couplings between $|k-1\rangle \leftrightarrow |k\rangle$ and $|k+1\rangle \leftrightarrow |k+2\rangle$. Both of these are first-order transitions with $n=1$ in Eq. (11). To address the two errors, two DRAG corrections can be introduced recursively [42, 48] as

$$\Omega_0 = \Omega_1 - i \frac{\dot{\Omega}_1}{\Delta_l}, \quad (17)$$

$$\Omega_1 = \Omega_2 - i \frac{\dot{\Omega}_2}{\Delta_h}, \quad (18)$$

where $\Delta_h = E_{|k+2\rangle} - E_{|k+1\rangle}$ and $\Delta_l = E_{|k\rangle} - E_{|k-1\rangle}$ are the upper and lower adjacent levels, respectively. For Ω_2 we use Ω_I in Eq. (15). The detailed derivation based on perturbation theory is provided in Appendix D. Each of these expressions is designed to address one leakage pathway, and their order is interchangeable due to the linearity of derivatives.

This is different from the high-order perturbative solution proposed in Ref. [41], where no second derivatives were introduced and the result is only a compromise between different errors. This recursive formulation suppresses both errors simultaneously to the leading order and can be extended with additional correction terms if more ancillary levels are involved [42]. Semiclassically, it can be understood as engineering two zero points on the classical spectrum of the pulse. We refer to this DRAG pulse as the DRAG2 pulse. Notably, for a weakly nonlinear oscillator where $\Delta_l \approx -\Delta_h$, the imaginary part of the correction becomes small, and the real part dominates:

$$\Omega_0 \approx \Omega_1 + \frac{\ddot{\Omega}_1}{\Delta_l^2} \approx \Omega_1 + \frac{\ddot{\Omega}_1}{\Delta_h^2}. \quad (19)$$

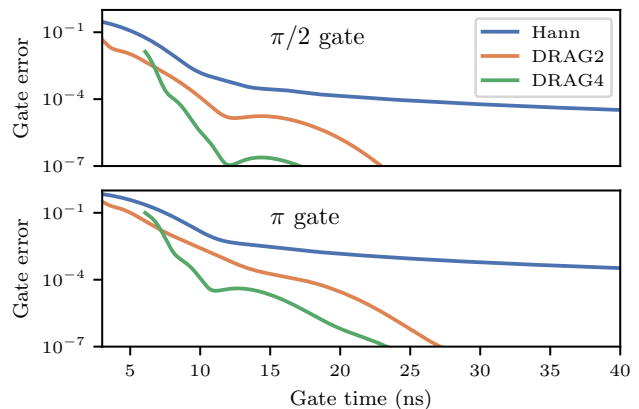


FIG. 4. Gate infidelity as a function of duration for different drive schemes driving the $|1\rangle \leftrightarrow |2\rangle$ transition, with $\alpha/(2\pi) = -200$ MHz and $\omega_{10}/(2\pi) = 5$ GHz. The DRAG2 pulse is defined in Equations (17) and (18) and the DRAG4 pulse in Equations (20) and (21).

Apart from the leakage error, two other errors, the phase and amplitude errors, must also be addressed to achieve the desired rotation. For a typical qubit operation between $|0\rangle \leftrightarrow |1\rangle$, the phase error comes from both the Stark shift caused by the $|2\rangle$ state and the non-commutativity of the imaginary DRAG correction term. For transitions involving higher levels, the Stark shift is influenced by both the higher and lower adjacent levels. Because the phase accumulation on the states $|k\rangle$ and $|k+1\rangle$ have the same sign, the overall accumulated phase error in this two-level transition is smaller compared to driving $|0\rangle \leftrightarrow |1\rangle$ [45]. Experimentally, this small phase error is often mitigated by applying a constant detuning to the drive [39]. The correction of the drive shape also affects the rotation angle. To compensate for this, a small correction term needs to be added, $\Omega_2 \leftarrow \Omega_2 + \Omega_{\text{amp}}$. Similar to the phase correction, this amplitude error can also be approximately mitigated by calibrating the maximal drive amplitude Ω_{\max} .

D. Second-order solution for qudits

Although the two couplings between $|k-1\rangle \leftrightarrow |k\rangle$ and $|k+1\rangle \leftrightarrow |k+2\rangle$ are suppressed by the DRAG2 correction, under a strong drive the higher-order transitions between $|k-1\rangle \leftrightarrow |k+1\rangle$ and $|k\rangle \leftrightarrow |k+2\rangle$ may also play a role. These second-order transitions arise from diagonalizing the direct ladder couplings and are proportional to Ω^2 (see Appendix D). Following the general DRAG expression in Eq. (14), this leads to the chained

second-order correction:

$$\Omega_2 = \sqrt{\Omega_3^2 - i \frac{2\Omega_3 \dot{\Omega}_3}{\Delta_h}} \quad (20)$$

$$\Omega_3 = \sqrt{\Omega_4^2 - i \frac{2\Omega_4 \dot{\Omega}_4}{\Delta_l}} \quad (21)$$

where Ω_4 is again taken from Ω_I in Eq. (15). We refer to this pulse, combined with the two corrections in Equations (17) and (18) as the DRAG4 pulse.

The second-order corrections introduced above commute with each other but do not commute with the first-derivative corrections. It is important to note that in the recursive DRAG formulation, the second-order correction is applied first to the initial pulse. This ensures that the dynamics in the final effective frame are governed by the initial pulse. This ordering is the reverse of the order of perturbation.

E. Performance benchmarking

To demonstrate the performance of the recursive DRAG pulse, we simulate the time evolution for various gate durations and compare different drive schemes. We use the analytically derived DRAG pulse while numerically calibrating constant detuning δ_d and amplitude Ω_{\max} . The simulation is performed using the full Hamiltonian, truncated at N_{\max} , which is much larger than the qudit size. The average gate fidelity is calculated as [57]

$$F[\hat{\mathcal{U}}_Q] = \frac{\text{Tr}[\hat{\mathcal{U}}_Q \hat{\mathcal{U}}_Q^\dagger]}{d(d+1)} + \frac{|\text{Tr}[\hat{\mathcal{U}}_Q \hat{\mathcal{U}}_I^\dagger]|^2}{d(d+1)}, \quad (22)$$

with $\hat{\mathcal{U}}_Q$ representing the truncated unitary within the two-level subspace for the targeted transition and $\hat{\mathcal{U}}_I$ the ideal π and $\pi/2$ rotation gates. Note that this fidelity only includes deviations in the gate quality within the two-level subspace and error leakages from the target states $|k\rangle$ and $|k+1\rangle$. Error dynamics that may occur on other levels are discussed in Section IV.

In Fig. 4, we compare the gate fidelity between standard Hann pulse, DRAG2 and DRAG4 pulses, for π and $\pi/2$ gates on $|1\rangle \leftrightarrow |2\rangle$. For short gate durations, below 25 ns, each successive correction improves fidelity by one to two orders of magnitude. For longer gate times, the error is primarily dominated by the phase and amplitude error, which are suppressed by the constant detuning and amplitude recalibration. The DRAG4 corrections are effective until the gate time is reduced to below 7 ns, where the ratio Ω_{\max}/Δ approaches one and the perturbative assumption breaks. This improvement can also be examined by fixing a target fidelity and examining the minimum gate time required to achieve it. For instance, with a target fidelity of 10^{-4} , the DRAG pulse reduces the gate duration to 10 ns from 30 ns for a $\pi/2$ gate, and from more than 40 ns to 15 ns for a π gate.

Generalizing the analysis to arbitrary $|k\rangle \leftrightarrow |k+1\rangle$ transitions, we apply the same DRAG construction and repeat the benchmarking for different k values. Fig. 5a shows the fidelity improvement for three different anharmonicities α and gate times. As the anharmonicity decreases, the system more closely resembles a linear oscillator, allowing more levels to be used as quantum registers without significant coupling to environmental noise. However, the energy difference between each level, roughly proportional to the anharmonicity, also decreases. Therefore, we increase the gate time proportionally, inversely to the reduced anharmonicity. The results indicate that the improvements provided by the DRAG corrections for general $|k\rangle$ transitions with varying anharmonicity are analogous to those observed for $|1\rangle \leftrightarrow |2\rangle$ in Fig. 4. This also verifies that the four-level effective model is well suited for studying the transmon ladder transition across different levels. In addition, we observe that control errors decrease as the level k increases, mainly because the leakage coupling to upper and lower levels becomes more symmetric as the level goes up. As the two leakage couplings $|k-1\rangle \leftrightarrow |k\rangle$ and $|k+1\rangle \leftrightarrow |k+2\rangle$ become more symmetric, the phase error is reduced for higher levels, as also observed in Ref. [45].

To further characterize the control of different ladder transitions, we compute the minimal gate duration achievable for a fidelity threshold of 10^{-4} , as depicted in Fig. 5b. To capture the universality of the pulse solutions, we normalize the time by the energy separation Δ_k for each ladder transition. Remarkably, we see that when comparing different transition indices k , and comparing different values of the anharmonicity, all the values collapse horizontally on the same line for the DRAG family of pulses. When we use DRAG4 pulses instead of DRAG2, we remove two additional weak, 2-photon transitions, and these collapse to a yet shorter minimum time line (related to a quantum speed limit for the particular choice of pulse), with apparently even stronger overlap for different parameters. However, this does not happen for the standard Hann pulse, where there is a strong dependence both on the anharmonicity (or equivalently E_J/E_C) and the chosen level index. We interpret this as evidence that removing the leakage transitions gives an effective qubit model with universal behaviour, independent of the nature of the leakage transitions themselves.

IV. ERROR BEYOND THE TARGETED TWO-LEVEL SUBSPACE

In the previous analysis, we focused on the relevant two-level subspace and computed the average gate fidelity of driving a π or $\pi/2$ rotation, using Eq. (22). For a target transition between $|k\rangle \leftrightarrow |k+1\rangle$, this error model includes leakage from the target subspace to $|k-1\rangle$ and $|k+2\rangle$ and the corresponding phase and amplitude error. To use it as the building block for universal qudit

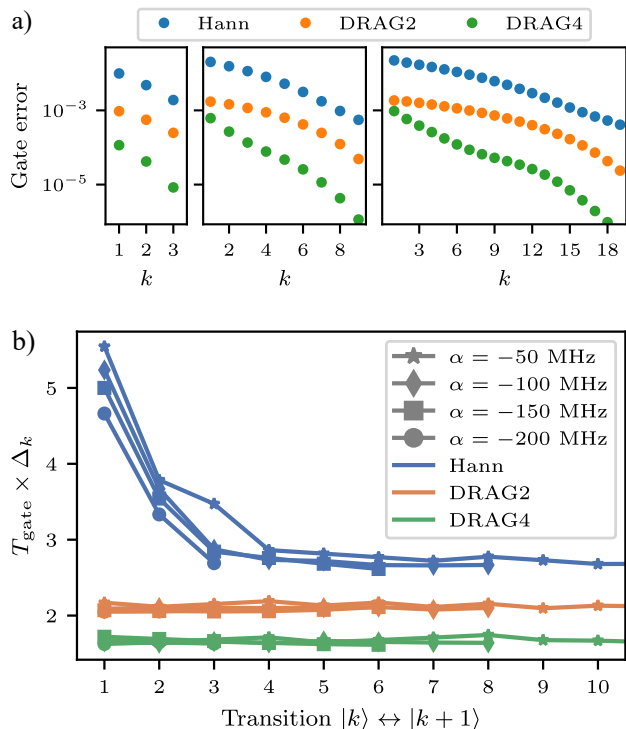


FIG. 5. Controlling the ladder transitions in a transmon qubit. a) The $\pi/2$ gate error for different ladder transitions $|k\rangle \leftrightarrow |k+1\rangle$ for $\alpha/(2\pi) = -200, -100, -50$ MHz using a fixed gate duration of 8, 15 and 30 ns respectively. These values of anharmonicity correspond to $E_C/E_J \approx 100, 355$ and 1331, respectively. b) The minimum gate time required to achieve fidelity of 10^{-4} for different drive schemes and different hardware parameters for a $\pi/2$ gate. The gate duration is multiplied by the corresponding leakage level separation Δ_k , resulting in overlapping outcomes across different hardware parameters and qubit levels.

computational gates, we also need to study its effect on all the K qubit states.

A. Phase error beyond the two target levels.

As discussed above, the Stark shift accumulates phases on the affected subspace. The optimized detuning fixes the difference between the phase on $|k\rangle$ and $|k+1\rangle$. However, a phase shift still exists between the subspace and other energy levels. For the target ladder transition, this phase shift is merely a global phase, but for a K -level qubit, it becomes relevant and must be accounted for.

Fortunately, this phase mismatch can be easily calibrated by applying virtual phase gates to each untargeted level [33]. The accumulated phase is calibrated by using a phase-amplification technique. For an operation $\text{RX}_{\pi/2}^{(k,k+1)}$, the state $(|k\rangle + |j\rangle)/\sqrt{2}$ is prepared, where $|j\rangle$ is the state not addressed by the gate. The gate is then applied $8n$ times, followed by a rotation of the system

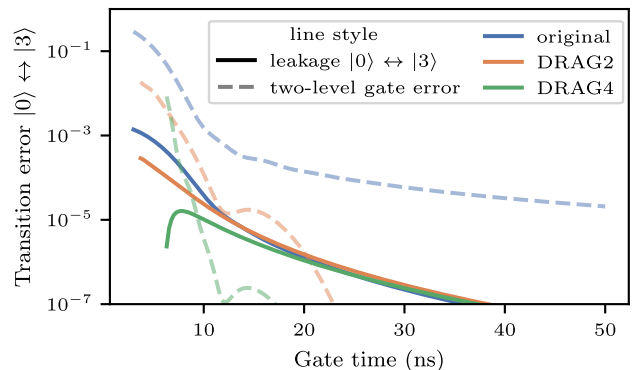


FIG. 6. The three-photon transition error under different drive schemes. The solid line represents the $|0\rangle \leftrightarrow |3\rangle$ error as a function of the gate time for different drive schemes for a $\pi/2$ gate. The dashed lines are the same as in Fig. 4 as a reference. The parameters used are also the same.

back using $\text{RY}_{\pi/2}^{(k,k+1)}$, similar to a Ramsey experiment. The accumulated phase is then measured on the state $|j\rangle$ and corrected for future use. Virtual phase gate construction is described in Appendix A2.

B. Leakage on $|k+2\rangle \leftrightarrow |k+3\rangle$

The DRAG pulse we studied primarily targets leakage involving the target subspace, i.e., leakage from the two target levels to the nearest neighbours, which are separated by approximately Δ_k in the rotating frame. Under a very strong drive, a small population transfer may also appear between nearby states such as $|k+2\rangle \leftrightarrow |k+3\rangle$, which are not directly driven. The level separation between them is about $2|\Delta_k|$. Due to this large separation, the unwanted transition is much smaller, however, it might become non-negligible ($> 10^{-4}$) if a DRAG4 pulse is used for a short gate time. Since they are small and do not involve the target states, a weak off-resonant drive can readily be added separately to cancel the small transition.

C. Three-photo leakage $|k-1\rangle \leftrightarrow |k+2\rangle$

Another small error that we have not discussed is the three-photon transition between $|k-1\rangle \leftrightarrow |k+2\rangle$. As illustrated in Fig. 1c, this third-order transition is induced by off-resonant ladder couplings and is proportional to Ω^3 . Although the absolute value of this error is accordingly small, due to the very small value of $\delta_{k-1,k+2}$ in a nonlinear oscillator, it may still introduce a non-negligible error after DRAG corrections. This error probability, defined by

$$\mathcal{L}_{k-1,k+2} = \frac{1}{4} \left(|\hat{U}_{k-1,k+2}|^2 + |\hat{U}_{k+2,k-1}|^2 \right) \quad (23)$$

the case of qubits, since there are $K - 1$ ladder transitions, we need to track the accumulated phase for each drive, which we denote as θ_k .

A rotation between $|k\rangle$ and $|k + 1\rangle$ is implemented by a Hamiltonian

$$\hat{H}_\Omega^{(k)}(\theta) = \begin{pmatrix} 0 & \frac{1}{2}e^{i\theta_k}\Omega(t) \\ \frac{1}{2}e^{-i\theta_k}\Omega(t) & 0 \end{pmatrix}, \quad (\text{A6})$$

where $\Omega(t)$ is the time dependent drive amplitude and θ a constant phase of the drive. This angle θ adjusts the axis in the XY plane, around which the rotation is performed. The corresponding unitary evolution is denoted by $\hat{U}_\Omega^{(k)}(\theta) = e^{-i\hat{H}_\Omega^{(k)}(\theta)t}$. It is then straightforward to show that

$$\text{RZ}^{(k,k+1)}(\phi)\hat{U}_\Omega^{(k)}(\theta) = \hat{U}_\Omega^{(k)}(\theta - \phi)\text{RZ}^{(k,k+1)}(\phi). \quad (\text{A7})$$

This relation indicates that by phase shifting the drive Ω by $-\phi$, the RZ phase gate can be effectively moved to the end of the gate operation. Since it appears at the end, it can be neglected, as measurements only capture state populations.

The above is enough for qubit operation. For qudit operation, however, the presence of other computational levels has to be taken into consideration. Therefore, we need to consider an RZ gate between arbitrary two levels and obtain the following expressions

$$\text{RZ}^{(j,k)}(\phi)\hat{U}_\Omega^{(k)}(\theta) = \hat{U}_\Omega^{(k)}(\theta + \phi/2)\text{RZ}^{(j,k)}(\phi), \quad (\text{A8})$$

$$\text{RZ}^{(k,l)}(\phi)\hat{U}_\Omega^{(k)}(\theta) = \hat{U}_\Omega^{(k)}(\theta - \phi/2)\text{RZ}^{(k,l)}(\phi), \quad (\text{A9})$$

$$\text{RZ}^{(j,k+1)}(\phi)\hat{U}_\Omega^{(k)}(\theta) = \hat{U}_\Omega^{(k)}(\theta - \phi/2)\text{RZ}^{(j,k+1)}(\phi), \quad (\text{A10})$$

$$\text{RZ}^{(k+1,l)}(\phi)\hat{U}_\Omega^{(k)}(\theta) = \hat{U}_\Omega^{(k)}(\theta + \phi/2)\text{RZ}^{(k+1,l)}(\phi), \quad (\text{A11})$$

with $j < k$ and $l > k + 1$. Notice that the adjusted phase is reduced by half because only one of the levels overlaps between RZ and the transition gate.

Appendix B: Transmon circuit in the charge representation

In this appendix, we will discuss a more general description of the transmon circuit that goes beyond the standard Duffing oscillator [53]. The fundamental aspect of this modelling is the representation of both charge and phase operators in Eq. (1). In the charge qubit description, the operator \hat{n} describes the excess of Cooper-Pair on the superconducting islands, while the cosine operator $\cos(\hat{\varphi})$ describes the tunnelling between them along the junction. Explicitly, we write:

$$\hat{n} := \sum_{n \in \mathbb{Z}} n |n\rangle\langle n|, \quad (\text{B1})$$

$$\exp(i\hat{\varphi}) := \sum_{n \in \mathbb{Z}} |n\rangle\langle n + 1|. \quad (\text{B2})$$

In this representation, the eigenstates of the transmon are obtained by numerically diagonalizing the Hamiltonian to a subspace spanned by a few charge states. This modifies the control operator \hat{n} in such a basis so that it exhibits selection rules different from the bosonic oscillator defining the Duffing oscillator [see Eq. (6)].

The gate voltage $n_g(t)$ responsible for driving the transitions on the transmon circuit is susceptible to fluctuations which could be thermal, due to wiring circuits and quasiparticle tunnelling through the junction, or non-thermal, due to impedance mismatching with the signal generator. Thus, we need to quantify the fluctuation of the energy levels of the transmon by varying $n_g(t)$. Fig. 7 shows the low-lying energy spectrum as a function of the gate voltage n_g . We have selected E_C and E_J such that the $\omega_{10}/(2\pi) = (\omega_1 - \omega_0)/(2\pi) = 5$ GHz, and we vary the anharmonicity $\alpha = \omega_{21} - 2\omega_{10}$ to be in the range $\alpha/(2\pi) = (-50, -300)$ (MHz).

We observe increasing charge dispersion for larger values of α . The main reason for the increase of charge dispersion with decreasing E_J relies on always the same frequency; consequently, fewer states are confined in the cosine potential. This feature is more appreciable when we see the variation of the energy spectrum $\partial\omega_{k+1,k}/\partial n_g$ with respect to the gate voltage, where for smaller α the fluctuations are on the order of KHz.

In this scenario, depending on our transmon parameters, we need to carefully select the workable low-lying energy levels for our qudit gates. In our case, we follow a different approach than Ref. [49]; rather than compute the ratio between the deep potential with the energy spacing, we consider the average of the fluctuation over n_g . In this work, we set a truncation at $\partial\omega_{N_{\max}}/\partial n_g \approx 10^{-3}$ (GHz) and consider any eigenstates with lower dispersion suitable as a qudit level. This results in the number of levels available in the nonlinear oscillator in Fig. 1.

This constraint on dispersion also extends to the dephasing time where we have used $1/f$ noise as the most detrimental source of decoherence which can be estimated by the relation [38, 61]

$$\frac{1}{T_\phi^{(k)}} = A_{n_g} \left| \frac{\partial\omega_{k+1,k}}{\partial n_g} \right| \sqrt{2|\ln(\omega_{\text{low}}t_{\text{exp}})|}, \quad (\text{B3})$$

where $\omega_{k+1,k} = \omega_{k+1} - \omega_k$ and $A_{n_g} = 10^{-4}e$ is the noise strength [62–64] with e being the electron charge. Also, $\omega_{\text{low}} = 2\pi/t_{\text{exp}}$ corresponds to the infrared cutoff due to the finite data acquisition time $t_{\text{exp}} = 10^4$ ns [38]

This is illustrated in Fig. 8, where one point corresponds to one qudit eigenstate with a specific hardware parameter. As the anharmonicity decreases, more and more levels with a coherence time longer than 100 μs can be included as quantum information registers.

For amplitude damping, we estimate T_1 assuming that the main loss mechanism corresponds to capacitive losses.

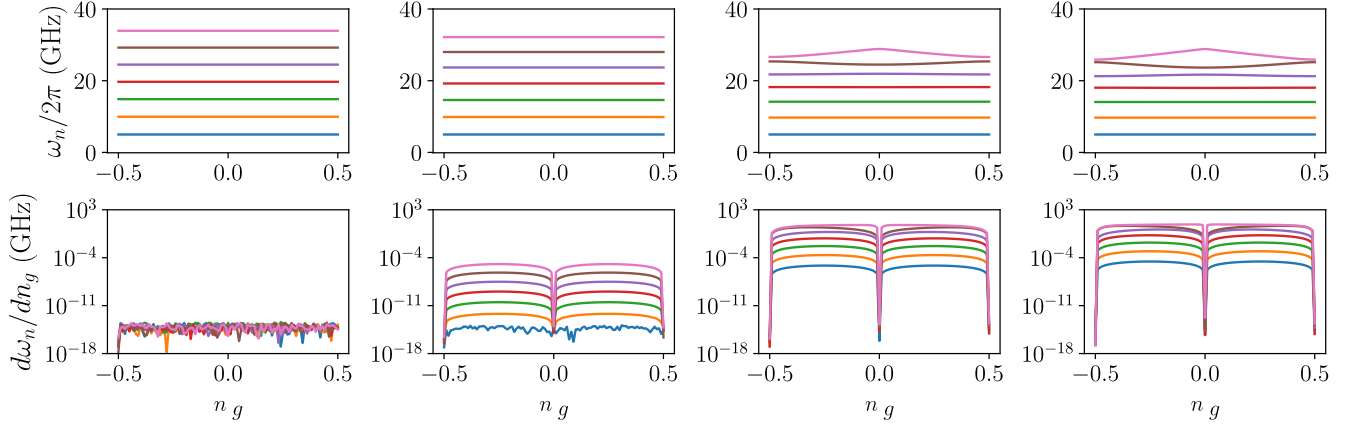


FIG. 7. Energy spectrum of the transmon circuit as a function of the dimensionless gate voltage n_g for four different values of $\alpha/(2\pi) = \{-50, -100, -200, -300\}$ (MHz). For the numerical simulations, we have fixed E_J for obtaining $\omega_{10}/(2\pi) = 5$ (GHz), and as expected, for increasing anharmonicity, the energy spectrum becomes more sensitive to charge fluctuations.

In such a way, Fermi's golden rules give the relation [65]

$$\frac{1}{T_1^{(k)}} = |\langle k | \hat{n} | k+1 \rangle|^2 S(\omega_{k+1,k}), \quad (\text{B4})$$

where the spectral density for the capacitive losses reads [61, 66]

$$S(\omega_{k+1,k}) = \frac{4\hbar E_C}{Q_{\text{cap}}(\omega_{k+1,k})} \left[\frac{\coth\left(\frac{\hbar|\omega_{k+1,k}|}{2k_B T}\right)}{1 + \exp\left(-\frac{\hbar\omega_{k+1,k}}{k_B T}\right)} \right] \quad (\text{B5})$$

with $Q_{\text{cap}}(\omega_{k+1,k}) = 10^6 (2\pi \times 6 \text{ GHz}/|\omega_{k+1,k}|)^{0.7}$ [67, 68] the capacitive quality factor per ladder transition. Also, k_B is the Boltzmann constant, and $T = 15$ mK is the temperature. Since this value is not strongly dependent on the levels in our system studied, we do not use it to truncate the qudit level.

For completeness, we plot the T_1 for the different energy levels in Fig. 8. We should note that improvement of the coherent times could be possible by implementing different fabrication techniques such as surface error mitigation [69, 70], changing the Niobium with Tantalum as the base superconductor [71, 72] or mitigating the micromotion of the circuitry [73], among other techniques. Such shielding on the transmon circuit leads to coherence times nearly in the millisecond scale.

Appendix C: Derivation of the Leakage manifold

Here, we will show that the energy diagram for any qudit gate between the states $(k+1, k)$ is represented as in Fig. 1c. In other words, if we want to implement this single qudit gate, there appears to be a nearly-resonant transition between the states $|k-1\rangle \leftrightarrow |k+2\rangle$. To do so, let us consider the explicit form of the energy of the

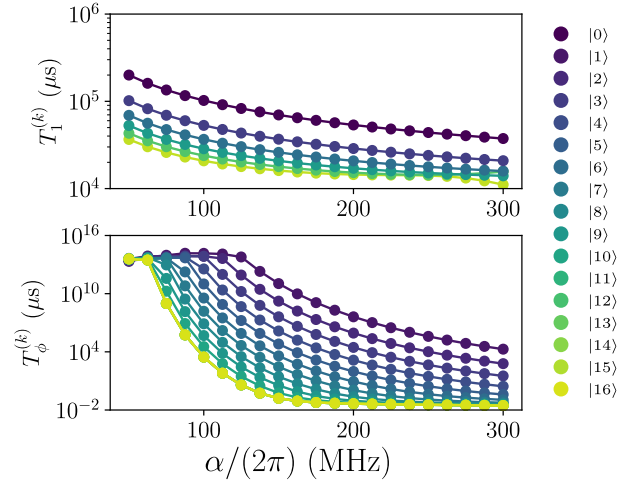


FIG. 8. Coherence times of the transmon circuit as a function of α for different transition frequency $\omega_{k+1,k}$. We set E_J and E_C such that the transition frequency equal to $\omega_{10}/(2\pi) = 5$ (GHz). For the amplitude damping, we assume capacitive losses and dephasing correspond to charge fluctuations.

k th energy level after the frame transformation in Eq. (7)

$$\tilde{\Delta}_k = \omega_k - k(\omega_{k+1} - \omega_k - \delta_d). \quad (\text{C1})$$

For the Dufing oscillator model, we know that $\omega_k = \omega - \alpha k(k-1)/2$, where $\omega = \sqrt{8E_C E_J} - E_C$ is the transmon frequency, and $\alpha = -E_C$ is the anharmonicity, respectively. Thus, $\tilde{\Delta}_{k-1} = (k-1)(\alpha(k+2) + 2\delta_d)/2$ while $\tilde{\Delta}_{k+2} = (k+2)(\alpha(k-1) + 2\delta_d)/2$. Thus, the detuning between these energy levels is $\delta_{k-1,k+2} = 3\delta_d$ for all values of k , which is zero if the drive is resonant.

However, such a description of the system Hamiltonian is only valid for larger E_J/E_C . Thus, for obtaining better estimation of the detuning, we consider the

eigenenergies of the transmon obtained by numerical diagonalizing Eq. (1). Fig. 2d shows $\delta_{k-1,k+2}$ as a function of the anharmonicity α for several ladder transitions at $n_g = 0$; from the figure we appreciate an inverse relation between the degeneracy of the leakage state with the anharmonicity, recovering the previous calculation result when $\alpha = -2\pi \times 50$ (MHz). Moreover, we also see an increase of such discrepancy with the qudit manifold to be addressed, this effect is mainly produced by the sensitivity of the energy spectrum to the charge noise (see Fig. 7).

Appendix D: Derivation of recursive DRAG pulse

1. Single-photon correction

In the following, we show the derivation of the recursive DRAG pulse shape designed to suppress the two single-photon transitions $|k-1\rangle \leftrightarrow |k\rangle$ and $|k+1\rangle \leftrightarrow |k+2\rangle$. Our general approach is to progressively derive the effective frame and the corresponding drive shapes to minimize the prevalent error. Throughout the calculation, we keep the perturbative correction up to the second order for all the terms with two exceptions: the matrix entry (0, 3), which characterizes a three-photon leakage due to the small energy separation, and the entry (1, 2), which describes the pulse amplitude correction. For those two, we keep the terms up to the third-order correction.

We start with the rotating frame Hamiltonian in Eq. (8)

$$\hat{H}_0 = \begin{pmatrix} -\Delta_l & \frac{\lambda_1 \bar{\Omega}_0}{2} & 0 & 0 \\ \frac{\lambda_1 \Omega_0}{2} & \delta_d & \frac{\lambda_2 \bar{\Omega}_0}{2} & 0 \\ 0 & \frac{\lambda_2 \Omega_0}{2} & 2\delta_d & \frac{\lambda_3 \bar{\Omega}_0}{2} \\ 0 & 0 & \frac{\lambda_3 \Omega_0}{2} & \Delta_h + 3\delta_d \end{pmatrix}, \quad (\text{D1})$$

where $\Delta_h = \Delta_k + \delta_{k-1,k+2}$ and $\Delta_l = -\Delta_k$. For ease of notation, we use $\lambda_1, \lambda_2, \lambda_3$ for λ_{k-1}, λ_k and λ_{k+1} in this section. We define the first transition targeting the single-photon leakage error, $|k+1\rangle \leftrightarrow |k+2\rangle$. For small δ_d , as is typical in the transmon regime, this is the largest leakage source (see Fig. 2). The frame transformation generator is given by

$$\hat{S}_{0 \rightarrow 1} = \begin{pmatrix} 0 & -\frac{\lambda_1 \bar{\Omega}_1}{2\Delta_h} & 0 & 0 \\ \frac{\lambda_1 \Omega_1}{2\Delta_h} & 0 & -\frac{\lambda_2 \bar{\Omega}_1}{2\Delta_h} & 0 \\ 0 & \frac{\lambda_2 \Omega_1}{2\Delta_h} & 0 & -\frac{\lambda_3 \bar{\Omega}_1}{2\Delta_h} \\ 0 & 0 & \frac{\lambda_3 \Omega_1}{2\Delta_h} & 0 \end{pmatrix}. \quad (\text{D2})$$

The denominator Δ_h is chosen such that in the effective

frame, the matrix entry (2, 3) is zero. In addition, $S_{0 \rightarrow 1}$ is chosen to be proportional to the control term in \hat{H}_0 ; this is designed in particular such that there is no derivative term Ω_1 in \hat{H}_1 [48]. After substituting the expression $\Omega_0 = \Omega_1 - i\frac{\Omega_1}{\Delta_h}$, we get \hat{H}_1 with the off-diagonal term

$$\hat{H}_1 - \hat{H}_{1,\text{diag}} = \begin{pmatrix} 0 & \frac{1}{2}\epsilon\lambda_{r1}\bar{\Omega}_1 & \frac{-\Delta_l\epsilon^2\lambda_1\lambda_2\bar{\Omega}_1^2}{8\Delta_h^2} & \epsilon^3\bar{\Omega}_{L03}^{(1)} \\ \frac{1}{2}\epsilon\lambda_{r1}\Omega_1 & 0 & \frac{\epsilon\lambda_2(\bar{\Omega}_1 + \epsilon^2\bar{\Omega}_c^{(1)})}{2} & \frac{\epsilon^2\lambda_2\lambda_3\bar{\Omega}_1^2}{8\Delta_h} \\ \frac{-\Delta_l\epsilon^2\lambda_1\lambda_2\bar{\Omega}_1^2}{8\Delta_h^2} & \frac{\epsilon\lambda_2(\Omega_1 + \epsilon^2\Omega_c^{(1)})}{2} & 0 & 0 \\ \epsilon^3\bar{\Omega}_{L03}^{(1)} & \frac{\epsilon^2\lambda_2\lambda_3\Omega_1^2}{8\Delta_h} & 0 & 0 \end{pmatrix}, \quad (\text{D3})$$

where $\Omega_c^{(1)}$ and $\Omega_{L03}^{(1)}$ denote the third order error to the drive amplitude in this frame and the three-photon leakage transition, which we do not explicitly use in the following calculation. Notice that in the effective frame, we obtain a renormalized leakage rate $\lambda_{r1}\Omega_1$ between $|k-1\rangle$ and $|k\rangle$, with $\lambda_{r1} = \lambda_1(1 - \Delta_l/\Delta_h) \approx 2\lambda_1$ in the limit $\delta_{k-1,k+2} \rightarrow 0$. This explains why the leakage increases with only one single derivative DRAG correction in Fig. 2b. This prefactor also needs to be taken into consideration when making perturbative assumptions. The diagonal energy terms are given by

$$E_{1,|k-1\rangle} = -\Delta_l - \frac{\lambda_1^2 \text{Re}(\Omega_0 \bar{\Omega}_1)}{2\Delta_h} + \frac{\lambda_1^2 \Delta_l |\Omega_1|^2}{4\Delta_h^2}, \quad (\text{D4})$$

$$E_{1,|k\rangle} = \delta_d + \left(\frac{\lambda_1^2 - \lambda_2^2}{2\Delta_h} \right) \text{Re}(\Omega_0 \bar{\Omega}_1) - \frac{\lambda_1^2 \Delta_l |\Omega_1|^2}{4\Delta_h^2}, \quad (\text{D5})$$

$$E_{1,|k+1\rangle} = 2\delta_d + \left(\frac{\lambda_2^2 - \lambda_3^2}{2\Delta_h} \right) \text{Re}(\Omega_0 \bar{\Omega}_1) + \frac{\lambda_3^2 |\Omega_1|^2}{4\Delta_h}, \quad (\text{D6})$$

$$E_{1,|k+2\rangle} = 3\delta_d + \Delta_h + \frac{\lambda_3^2 \text{Re}(\Omega_0 \bar{\Omega}_1)}{2\Delta_h} - \frac{\lambda_3^2 |\Omega_1|^2}{4\Delta_h}. \quad (\text{D7})$$

Secondly, we target the single photon leakage between state $|k-1\rangle$ and $|k\rangle$, with the frame transformation generator

$$\hat{S}_{1 \rightarrow 2} = \begin{pmatrix} 0 & -\frac{\epsilon\lambda_{r1}\bar{\Omega}_2}{2\Delta_l} & 0 & 0 \\ \frac{\epsilon\lambda_{r1}\Omega_2}{2\Delta_l} & 0 & -\frac{\epsilon\lambda_2\bar{\Omega}_2}{2\Delta_l} & 0 \\ 0 & \frac{\epsilon\lambda_2\Omega_2}{2\Delta_l} & 0 & 0 \\ 0 & 0 & 0 & 0 \end{pmatrix}. \quad (\text{D8})$$

This, together with the substitution $\Omega_1 = \Omega_2 - i\frac{\Omega_2}{\Delta_l}$, results in the suppression of the transition and gives \hat{H}_2

$$\hat{H}_2 - \hat{H}_{2,\text{diag}} = \begin{pmatrix} 0 & 0 & -\frac{\Delta_l \epsilon^2 \lambda_2 \bar{\Omega}_1^2}{8\Delta_h^2} - \frac{\epsilon^2 \lambda_2 \lambda_{r1} \bar{\Omega}_2^2}{8\Delta_l} & \bar{\Omega}_{L03}^{(1)} \\ 0 & 0 & \frac{\epsilon \lambda_2 (\bar{\Omega}_2 + \epsilon^2 \bar{\Omega}_c^{(2)})}{2} & \frac{\epsilon^2 \lambda_2 \lambda_3 \bar{\Omega}_1^2}{8\Delta_h} \\ -\frac{\Delta_l \epsilon^2 \lambda_2 \Omega_1^2}{8\Delta_h^2} - \frac{\epsilon^2 \lambda_2 \lambda_{r1} \Omega_2^2}{8\Delta_l} & \frac{\epsilon \lambda_2 (\Omega_2 + \epsilon^2 \Omega_c^{(2)})}{2} & 0 & 0 \\ \Omega_{L03}^{(1)} & \frac{\epsilon^2 \lambda_2 \lambda_3 \Omega_1^2}{8\Delta_h} & 0 & 0 \end{pmatrix}. \quad (\text{D9})$$

In addition to the leakage error, the phase error and the amplitude renormalization also need to be considered to get the desired rotation. The time-dependent phase correction is given by

$$\begin{aligned} \delta_d = & -\text{Re}(\Omega_1 \bar{\Omega}_2) \left(\frac{\lambda_2^2}{\Delta_l} - \frac{\lambda_{r1}^2}{2\Delta_l} \right) \\ & - \text{Re}(\Omega_0 \bar{\Omega}_1) \left(-\frac{\lambda_1^2}{2\Delta_h} + \frac{\lambda_2^2}{\Delta_h} - \frac{\lambda_3^2}{2\Delta_h} \right) \\ & - |\Omega_1|^2 \left(\frac{\Delta_l \lambda_1^2}{4\Delta_h^2} + \frac{\lambda_3^2}{4\Delta_h} \right) - \frac{|\Omega_2|^2 \lambda_{r1}^2}{4\Delta_l}, \end{aligned} \quad (\text{D10})$$

where $\lambda_{r1} = \lambda_1(1 - \Delta_l/\Delta_h)$.

Apart from that, the correction on the drive shape also slightly affects the rotation angle. A small correction term needs to be added $\Omega_2 \leftarrow \Omega_2 + \Omega_{\text{amp}}$. The analytical formula of the amplitude correction is written as

$$\begin{aligned} \Omega_{\text{amp}} = & \Omega_0 |\Omega_1|^2 \left(\frac{\lambda_1^2}{8\Delta_h^2} + \frac{\lambda_3^2}{8\Delta_h^2} - \frac{\lambda_2^2}{4\Delta_h^2} \right) \\ & + \Omega_1 |\Omega_2|^2 \left(\frac{\lambda_{r1}^2}{8\Delta_l^2} - \frac{\lambda_2^2}{4\Delta_l^2} \right) \\ & + \Omega_2 |\Omega_1|^2 \left(-\frac{\lambda_1^2}{4\Delta_h^2} - \frac{\lambda_3^2}{4\Delta_l \Delta_h} \right) \\ & + \Omega_2 \text{Re}(\Omega_0 \bar{\Omega}_1) \left(\frac{\lambda_1^2}{2\Delta_l \Delta_h} + \frac{\lambda_3^2}{2\Delta_l \Delta_h} - \frac{\lambda_2^2}{\Delta_l \Delta_h} \right) \\ & + \Omega_1^2 \bar{\Omega}_0 \left(\frac{\lambda_1^2}{8\Delta_h^2} + \frac{\lambda_3^2}{8\Delta_h^2} - \frac{\lambda_2^2}{4\Delta_h^2} \right) \\ & + \delta_d \left(-\frac{\Omega_1}{\Delta_h} - \frac{\Omega_2}{\Delta_l} \right) \\ & + \Omega_1^2 \bar{\Omega}_1 \left(-\frac{\Delta_l \lambda_1^2}{8\Delta_h^3} - \frac{\lambda_3^2}{8\Delta_h^2} \right) \\ & + \Omega_2^2 \bar{\Omega}_1 \left(\frac{\lambda_{r1}^2}{8\Delta_l^2} - \frac{\lambda_2^2}{4\Delta_l^2} \right) \\ & - \frac{\lambda_1 \Omega_1^2 \bar{\Omega}_2 \lambda_{r1}}{8\Delta_h^2} - \frac{\Omega_2^2 \bar{\Omega}_2 \lambda_{r1}^2}{8\Delta_l^2}. \end{aligned} \quad (\text{D11})$$

In our investigation, we neglect the time dependence and numerically optimize a fixed correction of the detuning and the amplitude.

2. Two-photon correction

The first two transitions yield the effective Hamiltonian described in Eq. (D9), where the desired transition between $|k\rangle \leftrightarrow |k+1\rangle$ is preserved, with a renormalized effective coupling strength. The diagonalization of the single-photon coupling introduces new two-photon transitions, $|k-1\rangle \leftrightarrow |k+1\rangle$ and $|k\rangle \leftrightarrow |k+2\rangle$, with the coupling strength proportional to Ω^2 . This is also obtained for qubit driving in a nonlinear oscillator, as discussed in [42]. For very strong drive amplitude, these two-photon transitions become the dominant source of error once the single-photon transitions are sufficiently suppressed.

For simplicity, we do not repeat the full calculation as in the last subsection but note the following properties. We can treat Ω^2 as the new coupling g , then derive the same expression to suppress the two leakages as in Eq. (18) but with the coupling g . Moreover, any perturbative diagonalization of the two-photon transitions will introduce corrections only in the order of ϵ^3 or smaller, which is negligible relative to the truncation order considered. By substituting g back into Ω , we obtain the expression in Eq. (21).

3. Three-photon correction

In principle, based on the DRAG2 pulse, we can follow a similar strategy and use a recursive DRAG design to suppress the transition error between state $|0\rangle$ and $|3\rangle$:

$$\Omega_4 = \sqrt[3]{\Omega_5^3 - i \frac{3\Omega_5^2 \dot{\Omega}_5}{\delta_{k-1,k+2}}}. \quad (\text{D12})$$

However, due to the small gap between $|k-1\rangle$ and $|k+2\rangle$ in the transmon regime, the imaginary DRAG correction term is much larger and a constant detuning may not suffice to compensate for the phase error. Nevertheless, even with a not perfectly aligned phase, a $\pi/2$ gate can be implemented with the help of virtual phase gates.

Alternatively, one could explore the direct coupling between the states $|k-1\rangle$ and $|k+2\rangle$ instead of relying on the multi-photon process. However, this would require microwave drive generators with a frequency approximately three times that of the qubit frequency.

ACKNOWLEDGMENTS

This work was funded by the Federal Ministry of Education and Research (BMBF) within the framework programme "Quantum technologies – from basic research to market" (Project QSolid, Grant No. 13N16149), by the Deutsche Forschungsgemeinschaft (DFG, German Research Foundation) under Germany's Excellence Strategy – Cluster of Excellence Matter and Light for Quantum Computing (ML4Q) EXC 2004/1 – 390534769, by HORIZON-CL4-2022-QUANTUM-01-SGA Project

under Grant 101113946 OpenSuperQPlus100 and the European Union's Horizon Programme (HORIZON-CL4-2021-DIGITALEMERGING-02-10) Grant Agreement 101080085 QCFD. A.L. acknowledges support from NSERC through the Discovery and Quantum Alliance International programs. The authors gratefully acknowledge the Gauss Centre for Supercomputing e.V. (www.gauss-centre.eu) for funding this project by providing computing time through the John von Neumann Institute for Computing (NIC) on the GCS Supercomputer JUWELS at Jülich Supercomputing Centre (JSC).

-
- [1] D. Gottesman, Fault-Tolerant Quantum Computation with Higher-Dimensional Systems, in *Quantum Computing and Quantum Communications*, Vol. 1509, edited by G. Goos, J. Hartmanis, J. Van Leeuwen, and C. P. Williams (Springer Berlin Heidelberg, Berlin, Heidelberg, 1999) pp. 302–313.
- [2] Y.-M. Di and H.-R. Wei, Optimal synthesis of multivalued quantum circuits, *Physical Review A* **92**, 062317 (2015).
- [3] F. Motzoi, M. P. Kaicher, and F. K. Wilhelm, Linear and Logarithmic Time Compositions of Quantum Many-Body Operators, *Physical Review Letters* **119**, 160503 (2017).
- [4] S. Cao, M. Bakr, G. Campanaro, S. D. Fasciati, J. Wills, D. Lall, B. Shteynas, V. Chidambaram, I. Runger, and P. Leek, Emulating two qubits with a four-level transmon qudit for variational quantum algorithms, *Quantum Science and Technology* **9**, 035003 (2024), arXiv:2303.04796 [quant-ph].
- [5] A. Galda, M. Cubeddu, N. Kanazawa, P. Narang, and N. Earnest-Noble, Implementing a Ternary Decomposition of the Toffoli Gate on Fixed-Frequency Transmon Qutrits (2021), arXiv:2109.00558 [quant-ph].
- [6] B. P. Lanyon, M. Barbieri, M. P. Almeida, T. Jennewein, T. C. Ralph, K. J. Resch, G. J. Pryde, J. L. O'Brien, A. Gilchrist, and A. G. White, Simplifying quantum logic using higher-dimensional Hilbert spaces, *Nature Physics* **5**, 134 (2009).
- [7] P. J. Ollitrault, G. Mazzola, and I. Tavernelli, Nonadiabatic molecular quantum dynamics with quantum computers, *Phys. Rev. Lett.* **125**, 260511 (2020).
- [8] A. Miessen, P. J. Ollitrault, and I. Tavernelli, Quantum algorithms for quantum dynamics: A performance study on the spin-boson model, *Phys. Rev. Res.* **3**, 043212 (2021).
- [9] E. Rico, M. Dalmonte, P. Zoller, D. Banerjee, M. Bögli, P. Stebler, and U.-J. Wiese, $So(3)$ "nuclear physics" with ultracold gases, *Annals of Physics* **393**, 466 (2018).
- [10] G. Mazzola, S. V. Mathis, G. Mazzola, and I. Tavernelli, Gauge-invariant quantum circuits for $u(1)$ and yang-mills lattice gauge theories, *Phys. Rev. Res.* **3**, 043209 (2021).
- [11] M. Meth, J. F. Haase, J. Zhang, C. Edmunds, L. Postler, A. Steiner, A. J. Jena, L. Dellantonio, R. Blatt, P. Zoller, T. Monz, P. Schindler, C. Muschik, and M. Ringbauer, Simulating 2D lattice gauge theories on a qudit quantum computer (2024), arXiv:2310.12110.
- [12] D. Bruś and C. Macchiavello, Optimal eavesdropping in cryptography with three-dimensional quantum states, *Phys. Rev. Lett.* **88**, 127901 (2002).
- [13] H. Bechmann-Pasquinucci and A. Peres, Quantum cryptography with 3-state systems, *Phys. Rev. Lett.* **85**, 3313 (2000).
- [14] M. Grace, C. Brif, H. Rabitz, I. Walmsley, R. Kosut, and D. Lidar, Encoding a qubit into multilevel subspaces, *New Journal of Physics* **8**, 35 (2006).
- [15] A. Chiesa, E. Macaluso, F. Petiziol, S. Wimberger, P. Santini, and S. Carretta, Molecular Nanomagnets as Qubits with Embedded Quantum-Error Correction, *The Journal of Physical Chemistry Letters* **11**, 8610 (2020).
- [16] E. T. Campbell, Enhanced Fault-Tolerant Quantum Computing in d -Level Systems, *Physical Review Letters* **113**, 230501 (2014).
- [17] P. J. Low, B. M. White, A. A. Cox, M. L. Day, and C. Senko, Practical trapped-ion protocols for universal qudit-based quantum computing, *Physical Review Research* **2**, 033128 (2020).
- [18] M. Ringbauer, M. Meth, L. Postler, R. Stricker, R. Blatt, P. Schindler, and T. Monz, A universal qudit quantum processor with trapped ions, *Nature Physics* **18**, 1053 (2022).
- [19] P. Hrmo, B. Wilhelm, L. Gerster, M. W. van Mourik, M. Huber, R. Blatt, P. Schindler, T. Monz, and M. Ringbauer, Native qudit entanglement in a trapped ion quantum processor, *Nature Communications* **14**, 2242 (2023).
- [20] P. J. Low, B. White, and C. Senko, Control and Readout of a 13-level Trapped Ion Qudit (2023), arXiv:2306.03340.
- [21] D. González-Cuadra, T. V. Zache, J. Carrasco, B. Kraus, and P. Zoller, Hardware Efficient Quantum Simulation of Non-Abelian Gauge Theories with Qudits on Rydberg Platforms, *Physical Review Letters* **129**, 160501 (2022).
- [22] R. Hussain, G. Allodi, A. Chiesa, E. Garlatti, D. Mitcov, A. Konstantatos, K. S. Pedersen, R. De Renzi, S. Piligkos, and S. Carretta, Coherent manipulation of a molecular In-based nuclear qudit coupled to an electron qubit, *Journal of the American Chemical Society* **140**, 9814 (2018), pMID: 30040890, <https://doi.org/10.1021/jacs.8b05934>.
- [23] M. Chizzini, L. Crippa, L. Zaccardi, E. Macaluso, S. Carretta, A. Chiesa, and P. Santini, Quantum error correction with molecular spin qudits, *Phys. Chem. Chem. Phys.* **24**, 20030 (2022).
- [24] H. Biard, E. Moreno-Pineda, M. Ruben, E. Bonet, W. Wernsdorfer, and F. Balestro, Increasing the Hilbert

- space dimension using a single coupled molecular spin, *Nature Communications* **12**, 4443 (2021).
- [25] M. Kues, C. Reimer, P. Roztock, L. R. Cortés, S. Sciara, B. Wetz, Y. Zhang, A. Cino, S. T. Chu, B. E. Little, D. J. Moss, L. Caspani, J. Azaña, and R. Morandotti, On-chip generation of high-dimensional entangled quantum states and their coherent control, *Nature* **546**, 622 (2017).
- [26] M. Erhard, M. Malik, M. Krenn, and A. Zeilinger, Experimental Greenberger–Horne–Zeilinger entanglement beyond qubits, *Nature Photonics* **12**, 759 (2018).
- [27] Y.-H. Luo, H.-S. Zhong, M. Erhard, X.-L. Wang, L.-C. Peng, M. Krenn, X. Jiang, L. Li, N.-L. Liu, C.-Y. Lu, A. Zeilinger, and J.-W. Pan, Quantum Teleportation in High Dimensions, *Physical Review Letters* **123**, 070505 (2019).
- [28] E. J. Davis, G. Bentsen, L. Homeier, T. Li, and M. H. Schleier-Smith, Photon-Mediated Spin-Exchange Dynamics of Spin-1 Atoms, *Physical Review Letters* **122**, 010405 (2019).
- [29] Y. Chi, J. Huang, Z. Zhang, J. Mao, Z. Zhou, X. Chen, C. Zhai, J. Bao, T. Dai, H. Yuan, M. Zhang, D. Dai, B. Tang, Y. Yang, Z. Li, Y. Ding, L. K. Oxenløwe, M. G. Thompson, J. L. O’Brien, Y. Li, Q. Gong, and J. Wang, A programmable qudit-based quantum processor, *Nature Communications* **13**, 1166 (2022).
- [30] M. S. Blok, V. V. Ramasesh, T. Schuster, K. O’Brien, J. M. Kreikebaum, D. Dahlen, A. Morvan, B. Yoshida, N. Y. Yao, and I. Siddiqi, Quantum Information Scrambling on a Superconducting Qutrit Processor, *Physical Review X* **11**, 021010 (2021).
- [31] P. Liu, R. Wang, J.-N. Zhang, Y. Zhang, X. Cai, H. Xu, Z. Li, J. Han, X. Li, G. Xue, W. Liu, L. You, Y. Jin, and H. Yu, Performing $SU(d)$ Operations and Rudimentary Algorithms in a Superconducting Transmon Qudit for $d = 3$ and $d = 4$, *Physical Review X* **13**, 021028 (2023).
- [32] E. Champion, Z. Wang, R. Parker, and M. Blok, Multi-frequency control and measurement of a spin-7/2 system encoded in a transmon qudit (2024), arXiv:2405.15857 [quant-ph].
- [33] A. Morvan, V. V. Ramasesh, M. S. Blok, J. M. Kreikebaum, K. O’Brien, L. Chen, B. K. Mitchell, R. K. Naik, D. I. Santiago, and I. Siddiqi, Qutrit Randomized Benchmarking, *Physical Review Letters* **126**, 210504 (2021).
- [34] M. A. Yurtalan, J. Shi, M. Kononenko, A. Lupascu, and S. Ashhab, Implementation of a Walsh-Hadamard Gate in a Superconducting Qutrit, *Physical Review Letters* **125**, 180504 (2020).
- [35] M. Kononenko, M. A. Yurtalan, S. Ren, J. Shi, S. Ashhab, and A. Lupascu, Characterization of control in a superconducting qutrit using randomized benchmarking, *Physical Review Research* **3**, L042007 (2021).
- [36] M. Yurtalan, J. Shi, G. Flatt, and A. Lupascu, Characterization of Multilevel Dynamics and Decoherence in a High-Anharmonicity Capacitively Shunted Flux Circuit, *Physical Review Applied* **16**, 054051 (2021).
- [37] K. Luo, W. Huang, Z. Tao, L. Zhang, Y. Zhou, J. Chu, W. Liu, B. Wang, J. Cui, S. Liu, F. Yan, M.-H. Yung, Y. Chen, T. Yan, and D. Yu, Experimental Realization of Two Qutrits Gate with Tunable Coupling in Superconducting Circuits, *Physical Review Letters* **130**, 030603 (2023).
- [38] J. Koch, T. M. Yu, J. Gambetta, A. A. Houck, D. I. Schuster, J. Majer, A. Blais, M. H. Devoret, S. M. Girvin, and R. J. Schoelkopf, Charge-insensitive qubit design derived from the Cooper pair box, *Physical Review A* **76**, 042319 (2007).
- [39] Z. Chen, J. Kelly, C. Quintana, R. Barends, A. N. Korotkov, J. M. Martinis, *et al.*, Measuring and Suppressing Quantum State Leakage in a Superconducting Qubit, *Physical Review Letters* **116**, 020501 (2016).
- [40] F. Motzoi, J. M. Gambetta, P. Rebentrost, and F. K. Wilhelm, Simple Pulses for Elimination of Leakage in Weakly Nonlinear Qubits, *Physical Review Letters* **103**, 110501 (2009).
- [41] J. M. Gambetta, F. Motzoi, S. T. Merkel, and F. K. Wilhelm, Analytic control methods for high-fidelity unitary operations in a weakly nonlinear oscillator, *Physical Review A* **83**, 012308 (2011).
- [42] F. Motzoi and F. K. Wilhelm, Improving frequency selection of driven pulses using derivative-based transition suppression, *Physical Review A* **88**, 062318 (2013).
- [43] L. S. Theis, F. Motzoi, S. Machnes, and F. K. Wilhelm, Counteracting systems of diabaticities using DRAG controls: The status after 10 years, *EPL (Europhysics Letters)* **123**, 60001 (2018).
- [44] J. M. Chow, L. DiCarlo, J. M. Gambetta, F. Motzoi, L. Frunzio, S. M. Girvin, and R. J. Schoelkopf, Optimized driving of superconducting artificial atoms for improved single-qubit gates, *Physical Review A* **82**, 040305 (2010).
- [45] E. Lucero, J. Kelly, R. C. Bialczak, M. Lenander, M. Mariantoni, M. Neeley, A. D. O’Connell, D. Sank, H. Wang, M. Weides, J. Wenner, T. Yamamoto, A. N. Cleland, and J. M. Martinis, Reduced phase error through optimized control of a superconducting qubit, *Physical Review A* **82**, 042339 (2010).
- [46] L. DiCarlo, J. M. Chow, J. M. Gambetta, L. S. Bishop, B. R. Johnson, D. I. Schuster, J. Majer, A. Blais, L. Frunzio, S. M. Girvin, and R. J. Schoelkopf, Demonstration of two-qubit algorithms with a superconducting quantum processor, *Nature* **460**, 240 (2009).
- [47] K. X. Wei, E. Magesan, I. Lauer, S. Srinivasan, D. F. Bogorin, S. Carnevale, G. A. Keefe, Y. Kim, D. Klaus, W. Landers, N. Sundaresan, C. Wang, E. J. Zhang, M. Steffen, O. E. Dial, D. C. McKay, and A. Kandala, Hamiltonian Engineering with Multicolor Drives for Fast Entangling Gates and Quantum Crosstalk Cancellation, *Physical Review Letters* **129**, 060501 (2022).
- [48] B. Li, T. Calarco, and F. Motzoi, Experimental error suppression in Cross-Resonance gates via multi-derivative pulse shaping, *npj Quantum Information* **10**, 1 (2024).
- [49] Z. Wang, R. W. Parker, E. Champion, and M. S. Blok, Systematic study of high e_j/e_c transmon qudits up to $d = 12$ (2024), arXiv:2407.17407 [quant-ph].
- [50] D. C. McKay, C. J. Wood, S. Sheldon, J. M. Chow, and J. M. Gambetta, Efficient Z gates for quantum computing, *Physical Review A* **96**, 022330 (2017).
- [51] F. Preti, T. Calarco, and F. Motzoi, Continuous quantum gate sets and pulse class meta-optimization (2022), arXiv:2203.13594 [quant-ph].
- [52] B. Khani, J. M. Gambetta, F. Motzoi, and F. K. Wilhelm, Optimal generation of Fock states in a weakly nonlinear oscillator, *Physica Scripta* **2009**, 014021 (2009).
- [53] A. Blais, A. L. Grimsmo, S. M. Girvin, and A. Wallraff, Circuit Quantum Electrodynamics, *Reviews of Modern Physics* **93**, 025005 (2021), arXiv:2005.12667 [quant-ph].
- [54] V. Tripathi, N. Goss, A. Vezvae, L. B. Nguyen, I. Siddiqi, and D. A. Lidar, Qudit Dynamical Decou-

- pling on a Superconducting Quantum Processor (2024), arXiv:2407.04893 [quant-ph].
- [55] F. Motzoi, *Controlling Quantum Information Devices*, Ph.D. thesis, University of Waterloo (2012).
- [56] M. Deschamps, G. Kervern, D. Massiot, G. Pintacuda, L. Emsley, and P. J. Grandinetti, Superadiabaticity in magnetic resonance, *The Journal of Chemical Physics* **129**, 204110 (2008).
- [57] L. H. Pedersen, N. M. Møller, and K. Mølmer, Fidelity of quantum operations, *Physics Letters A* **367**, 47 (2007).
- [58] E. Hyppä, A. Vepsäläinen, M. Papič, C. F. Chan, S. Inel, A. Landra, W. Liu, J. Luus, F. Marxer, C. Ockeloen-Korppi, S. Orbell, B. Tarasinski, and J. Heinsoo, Reducing leakage of single-qubit gates for superconducting quantum processors using analytical control pulse envelopes (2024), arXiv:2402.17757 [quant-ph].
- [59] V. Ramakrishna, R. Ober, X. Sun, O. Steuernagel, J. Botina, and H. Rabitz, Explicit generation of unitary transformations in a single atom or molecule, *Physical Review A* **61**, 032106 (2000).
- [60] G. K. Brennen, D. P. O’Leary, and S. S. Bullock, Criteria for Exact Qudit Universality, *Physical Review A* **71**, 052318 (2005), arXiv:quant-ph/0407223.
- [61] G. Ithier, E. Collin, P. Joyez, P. J. Meeson, D. Vion, D. Esteve, F. Chiarello, A. Shnirman, Y. Makhlin, J. Schrieffer, and G. Schön, Decoherence in a superconducting quantum bit circuit, *Phys. Rev. B* **72**, 134519 (2005).
- [62] O. Astafiev, Y. A. Pashkin, Y. Nakamura, T. Yamamoto, and J. S. Tsai, Quantum noise in the Josephson charge qubit, *Phys. Rev. Lett.* **93**, 267007 (2004).
- [63] A. B. Zorin, F.-J. Ahlers, J. Niemeyer, T. Weimann, H. Wolf, V. A. Krupenin, and S. V. Lotkhov, Background charge noise in metallic single-electron tunneling devices, *Phys. Rev. B* **53**, 13682 (1996).
- [64] B. G. Christensen, C. D. Wilen, A. Opremcak, J. Nelson, F. Schlenker, C. H. Zimonick, L. Faoro, L. B. Ioffe, Y. J. Rosen, J. L. DuBois, B. L. T. Plourde, and R. McDermott, Anomalous charge noise in superconducting qubits, *Phys. Rev. B* **100**, 140503 (2019).
- [65] W. Smith, A. Kou, X. Xiao, U. Vool, and M. Devoret, Superconducting circuit protected by two-cooper-pair tunneling, *npj Quantum Information* **6**, 8 (2020).
- [66] H. Zhang, S. Chakram, T. Roy, N. Earnest, Y. Lu, Z. Huang, D. K. Weiss, J. Koch, and D. I. Schuster, Universal fast-flux control of a coherent, low-frequency qubit, *Phys. Rev. X* **11**, 011010 (2021).
- [67] V. Braginsky, V. Ilchenko, and K. Bagdassarov, Experimental observation of fundamental microwave absorption in high-quality dielectric crystals, *Physics Letters A* **120**, 300 (1987).
- [68] C. Wang, C. Axline, Y. Y. Gao, T. Brecht, Y. Chu, L. Frunzio, M. H. Devoret, and R. J. Schoelkopf, Surface participation and dielectric loss in superconducting qubits, *Applied Physics Letters* **107**, 162601 (2015).
- [69] A. P. Place, L. V. Rodgers, P. Mundada, B. M. Smitham, M. Fitzpatrick, Z. Leng, A. Premkumar, J. Bryon, A. Vrajitoarea, S. Sussman, *et al.*, New material platform for superconducting transmon qubits with coherence times exceeding 0.3 milliseconds, *Nature Communications* **12**, 1779 (2021).
- [70] M. Tuokkola, Y. Sunada, H. Kivijärvi, L. Grönberg, J.-P. Kaikkonen, V. Vesterinen, J. Govenius, and M. Möttönen, Methods to achieve near-millisecond energy relaxation and dephasing times for a superconducting transmon qubit (2024), arXiv:2407.18778 [quant-ph].
- [71] C. Wang, X. Li, H. Xu, Z. Li, J. Wang, Z. Yang, Z. Mi, X. Liang, T. Su, C. Yang, G. Wang, W. Wang, Y. Li, M. Chen, C. Li, K. Linghu, J. Han, Y. Zhang, Y. Feng, Y. Song, T. Ma, J. Zhang, R. Wang, P. Zhao, W. Liu, G. Xue, Y. Jin, and H. Yu, Towards practical quantum computers: Transmon qubit with a lifetime approaching 0.5 milliseconds, *npj Quantum Information* **8**, 3 (2022).
- [72] M. Bal, A. A. Murthy, S. Zhu, F. Crisa, X. You, Z. Huang, T. Roy, J. Lee, D. v. Zanten, R. Pilipenko, *et al.*, Systematic improvements in transmon qubit coherence enabled by niobium surface encapsulation, *npj Quantum Information* **10**, 43 (2024).
- [73] S. Kono, J. Pan, M. Chegnizadeh, X. Wang, A. Youssefi, M. Scigliuzzo, and T. J. Kippenberg, Mechanically induced correlated errors on superconducting qubits with relaxation times exceeding 0.4 ms, *Nature Communications* **15**, 3950 (2024).